Journal of Computational Physics **181,** 545–563 (2002)
doi:10.1006/jcph.2002.7141

# A Semi-implicit Method for Resolution of Acoustic Waves in Low Mach Number Flows[1]

Clifton Wall, Charles D. Pierce, and Parviz Moin

*Department of Mechanical Engineering, Stanford University, Stanford, California 94305-3030*
E-mail: cwall@stanford.edu

Received June 18, 2001; revised May 1, 2002

A semi-implicit numerical method for time accurate simulation of compressible flow is presented. By extending the low Mach number pressure correction method, a Helmholtz equation for pressure is obtained in the case of compressible flow. The method avoids the acoustic CFL limitation, allowing a time step restricted only by the convective velocity, resulting in significant efficiency gains. Use of a discretization that is centered in both time and space results in zero artificial damping of acoustic waves. The method is attractive for problems in which Mach numbers are low, and the acoustic waves of most interest are those having low frequency, such as acoustic combustion instabilities. Both of these characteristics suggest the use of time steps larger than those allowable by an acoustic CFL limitation. In some cases it may be desirable to include a small amount of numerical dissipation to eliminate oscillations due to small-wavelength, high-frequency, acoustic modes, which are not of interest; therefore, a provision for doing this in a controlled manner is included in the method. Results of the method for several model problems are presented, and the performance of the method in a large eddy simulation is examined. 

*Key Words:* compressible flow; acoustics; pressure correction; combusiton instability.

## 1. INTRODUCTION

In simulations of flows at low Mach number, the incompressible Navier–Stokes equations are typically solved instead of the compressible equations. This results in significant computational savings, since the time step is limited only by the convective velocity and not the acoustic velocity. Although this approach saves computational effort, it eliminates

[1] This paper is dedicated to the memory of Charles D. Pierce (1969–2002), whose ideas were the inspiration for this work, and who continues be an inspiration to all who worked with him in the turbulent combustion community.



0021-9991/02 $35.00

acoustic waves from the problem, which may be important in some applications. To capture acoustic waves in a simulation, the compressible equations must be solved.

Traditional explicit schemes for simulation of compressible flow are limited to time steps that satisfy a CFL condition based on the sum of the acoustic and convective velocities. This leads to a severe restriction on the allowable time step at low Mach number. Several classes of methods have been developed which avoid the acoustic CFL restriction by using an implicit time advancement scheme. The first class is based on the splitting of the Navier–Stokes equations given by Strang [1]. Another class of methods is based on the extension of the pressure-correction approach to compressible flows [2–5], while the third class of methods uses dual time stepping integration [6–13]. Although implicit time advancement methods avoid the acoustic CFL restriction, they can introduce significant artificial damping of acoustic waves. This damping is a desirable property if the methods are used to find steady solutions for compressible flow, but it can lead to high resolution requirements to limit this damping if the methods are used for time-accurate simulation of acoustic waves.

In this paper, a pressure correction method is derived which avoids the acoustic CFL limitation and causes no artificial damping of acoustic waves. This makes the method attractive for simulation of flows at low Mach number in which low-frequency acoustic waves are important. In such flows, significant efficiency gains can be achieved by using large time steps, while the acoustic waves of interest will still be resolved. Analysis of the method in the case of linear acoustics and results of several other test cases are presented. The performance of the method when used for a large eddy simulation (LES) is also examined.

## 2. NUMERICAL METHOD

The equations to be solved are the continuity, momentum, and energy equations as well as the equation of state:

$$\frac{\partial \rho}{\partial t} + \frac{\partial \rho u_i}{\partial x_i} = 0, \tag{1}$$

$$\frac{\partial \rho u_i}{\partial t} + \frac{\partial \rho u_i u_j}{\partial x_j} = -\frac{\partial P}{\partial x_i} + \frac{\partial \tau_{ij}}{\partial x_j}, \tag{2}$$

$$\frac{\partial \rho h}{\partial t} + \frac{\partial \rho u_j h}{\partial x_j} = \frac{\partial}{\partial x_j}\left(k\frac{\partial T}{\partial x_j}\right) + \tau_{ij}\frac{\partial u_i}{\partial x_j} + \frac{\partial P}{\partial t} + u_j\frac{\partial P}{\partial x_j}, \tag{3}$$

$$\rho = \rho(P, h), \tag{4}$$

$$P = \rho R T. \tag{5}$$

In these equations $\rho$ is density, $u_i$ are the components of velocity, $P$ is pressure, $T$ is temperature, $h$ is enthalpy, $\tau$ is the viscous stress, and $R$ is the ideal gas constant. The enthalpy equation may be replaced by an equation for any other scalar variable (entropy, internal energy, etc.), which, along with pressure, completely specifies the thermodynamic state. The choice to solve an equation for a thermodynamic property has been made, because the pressure-correction equation, as will be shown in this section, contains a partial derivative of density with respect to pressure at a constant value of the scalar for which Eq. (3) is solved. For this partial derivative to exist, the scalar must be a thermodynamic property. A total energy equation would have better conservation properties in the presence of shocks, but

the present method is proposed for simulations of flow at low Mach number, where shocks are not an issue.

The equations are discretized in the following manner. Each velocity component is staggered in space by one-half grid point with respect to the scalar variables, $\rho$, $P$, and $h$ [14]. Additionally, all velocity components are staggered in time by one-half time step with respect to the scalar variables. At each time step, the velocity components, $u_i$, at $t^n$ and the scalar variables at $t^{n+1/2}$ are known, and the values of $u_i$ at $t^{n+1}$ and the scalar variables at $t^{n+3/2}$ are to be determined. (Half indices are used to denote temporal locations that are staggered by one-half time step with respect to integer indices.) This staggering is presented in Pierce [16] and leads to a more accurate and stable discretization of the time-dependent continuity equation. When expressing the fully discretized equations, difference and interpolation operators [15] are used to simplify notation. For example, the difference and interpolation operations in the $x_1$ coordinate direction would be given by

$$\delta_{x_1}(u) = \frac{u_{i+1,j,k} - u_{i,j,k}}{\Delta x} \tag{6}$$

and

$$\bar{u}^{x_1} = \frac{u_{i+1,j,k} + u_{i,j,k}}{2}, \tag{7}$$

respectively. Difference and interpolation operators in time are defined analogously and are given by the symbols $\delta_t(u)$ and $\bar{u}^t$. Note that when these definitions are used to express discretized tensorial equations, the convention of summing repeated indices will not apply to the superscripts on the interpolation operators. If the difference and interpolation operators are to be second-order accurate, then the results produced must be located at the midpoint between the original variables. When this staggered shifting is properly taken into account, this notation can be used to write the discrete equations in an index-free form, with the convention that any two quantities that are added or multiplied must be at the same location on the space–time grid.

The expression of the discretized governing equations will be simplified by introducing the intermediate variable $g_i$ for the momentum per unit volume, which is defined according to

$$g_i = \overline{\bar{\rho}^{x_i}}^t u_i, \quad u_i = g_i / \overline{\bar{\rho}^{x_i}}^t. \tag{8}$$

In this notation, the discrete continuity equation is

$$\delta_t(\rho) + \delta_{x_j}(g_j) = 0. \tag{9}$$

Note that this equation is both implicit and centered in both space and time. The discrete momentum equation is

$$\delta_t(g_i) + \delta_{x_j}\left(\overline{\overline{g_j}^{x_i}}^t \overline{\overline{u_i}^{x_j}}^t\right) = -\delta_{x_i}\left(\overline{\bar{P}^t}^t\right) + \delta_{x_j}(\tau_{ij}), \tag{10}$$

$$\tau_{ij} = \begin{cases} \overline{\bar{\mu}^{x_i}}^{x_j}\left[\delta_{x_j}\left(\overline{u_i}^t\right) + \delta_{x_i}\left(\overline{u_j}^t\right)\right], & i \neq j, \\ (2\mu + \lambda)\delta_{x_j}\left(\overline{u_i}^t\right), & i = j. \end{cases} \tag{11}$$

The momentum equation is also implicit and centered in space and time. The discretized enthalpy equation is

$$\delta_t(\rho h) + \delta_{x_j}\left(g_j \overline{\bar{h}^{x_j}}^{t}\right) = \delta_{x_j}\left(\overline{\bar{k}^{x_j}}^{t}\delta x_j \bar{T}^{t}\right) + \delta_t(P) + \overline{u_j \delta_{x_j}\bar{P}^{t}}^{x_j}, \tag{12}$$

which is also centered in space and time. In this equation, the viscous heating term has been neglected, which is appropriate at low Mach number.

This discretization is nearly identical to the discretization of Pierce [16], who performed large eddy simulations of the low Mach number, variable-density equations for reacting flow. Pierce's discretization has been shown to conserve kinetic energy exactly in the limit of constant density, while some previous authors have neglected the effects of time stepping in describing the conservation properties of their methods. In the case of variable-density flow Pierce's method does not conserve kinetic energy exactly, but it can be shown that the error terms in the kinetic energy equation are dependant on time step only and not grid spacing.

The first modification for the present formulation is to interpolate the pressure in time twice, $\overline{\bar{P}^{t}}^{t}$, before inserting it into the momentum equations. In conventional notation, this means that the velocity is advanced from $t^n$ to $t^{n+1}$ using the gradient of a weighted average of pressure at times $t^{n-1/2}$, $t^{n+1/2}$, and $t^{n+3/2}$:

$$\overline{\bar{P}^{t}}^{t} = \frac{P^{n-1/2} + 2P^{n+1/2} + P^{n+3/2}}{4}. \tag{13}$$

This extra interpolation is necessary to make the pressure gradient term implicit and, therefore, to eliminate the acoustic CFL requirement. The other differences between the present formulation and that of Pierce [16] are the solution of the enthalpy equation and the evaluation of density from an equation of state which depends on local values of both pressure and enthalpy.

In practice it may be desirable to add a small amount of dissipation to prevent point-to-point oscillations in the solution due to high-wavenumber acoustic modes. If such acoustic modes are generated and are not dissipated, small-scale oscillations, which may not be physical, will appear. To prevent such oscillations, when necessary, $\overline{\bar{P}^{t}}^{t}$ in the pressure gradient term of the discrete momentum equation can be replaced by $\overline{\bar{P}^{t}}^{t*}$, defined as

$$\overline{\bar{P}^{t}}^{t*} = \left(\frac{1}{4} - \epsilon\right)P^{n-1/2} + \frac{1}{2}P^{n+1/2} + \left(\frac{1}{4} + \epsilon\right)P^{n+3/2}. \tag{14}$$

For $\epsilon > 0$, this change will bias the pressure gradient term toward its future value and will, therefore, have a dissipative effect, similar to the effect of upwinding in spatial discretization. This change will have the greatest effect on the smallest scales in the calculation; therefore, $\epsilon$ can be adjusted to a level that will achieve the desired dissipation on the small scales, while having little effect on the large scales, which are of interest. It will be shown in Section 4.4 that a very small value of $\epsilon$ (e.g., 0.005) is sufficient for an actual turbulent flow simulation. The scheme can formally be shown to maintain its second-order accuracy in time, as long as $\epsilon$ is chosen to be a function of $\Delta t$, which is proportional to $\Delta t$ in the limit of $\Delta t$ becoming arbitrarily small. There is no reason to maintain this proportionality in the limit of large $\Delta t$, so it is recommended that $\epsilon$ be bounded by a finite value in this limit. If such a dependence on $\Delta t$ is chosen, $\epsilon$ will perform a similar role to the artificial diffusion term in stabilized

finite element methods [17, 18]. In these methods a similar modification is made to the spatial discretization to achieve a desired level of numerical dissipation without causing excessive dissipation of the scales of interest or lowering the formal order of accuracy.

Although all terms in the preceding equations are treated implicitly, achieving stability independent of the acoustic CFL number requires only that the continuity equation, the pressure gradient term in the momentum equations, and the pressure work term in the energy equation be treated in this manner [19]. Centered discretizations in space and time of the continuity equation and the pressure gradient term in the momentum equations gives the method zero dissipation of acoustic waves as long as dissipation is not added by the use of $\overline{\bar{P}^t}^{t*}$. The reason for this will be shown in the analysis of the method for the case of linear acoustics. It should be noted that the staggered variable arrangement is not necessary to achieve this centering in space and time and that a version of this method for a collocated variable arrangement can be derived similarly; however, the analysis and results presented here are for the staggered version and may not be directly applied to a collocated version.

This implicit system of equations has excellent stability properties. In practice, these equations are solved iteratively with a finite number of iterations and the solution can be considered to be semi-implicit. However, if a sufficient number of iterations are performed, this semi-implicit method is more efficient and still retains nearly the same stability properties as an implicit method.

The algorithm for obtaining the solution to this system of discrete equations is similar to the pressure-correction method for incompressible flow. The steps of the method are given in the following steps . In this description, the first superscript $n$, denotes the time step, and the second superscript, $k$, denotes iteration number. Variables which do not have a superscript indicating iteration number refer to the value at the end of the iteration process.

*Step 1: Choose predictors.* Initial guesses for the value of all variables at the new time step are taken to be the values at the current time step:

$$u_i^{n+1,0} = u_i^n, \quad \rho^{n+3/2,0} = \rho^{n+1/2}, \quad h^{n+3/2,0} = h^{n+1/2}, \text{ etc.} \tag{15}$$

*Step 2: Advance scalar.* The first step within each iteration loop is to advance the enthalpy. Advancement of Eq. (12) yields $(\rho h)^{n+3/2,k+1}$, from which $h^{n+3/2,k+1}$ is obtained by dividing by the current estimate of density at the new time step, $\rho^{n+3/2,k}$.

*Step 3: Evaluate equation of state.* The density is evaluated from the equation of state,

$$\tilde{\rho}^{n+3/2,k+1} = \rho\left(P^{n+3/2,k}, h^{n+3/2,k+1}\right). \tag{16}$$

A tilde on this value of $\rho$ is used to note that it is only a provisional value and will be updated again using a more accurate value of pressure before the end of the iteration.

*Step 4: Advance velocity.* The momentum equations are advanced to yield a provisional value of the momentum per unit volume, $\tilde{g}_i^{n+1,k+1}$. This value is provisional, because it has been computed using the current iterate of pressure, $P^{n+3/2,k}$, and will later be corrected to account for the new iterate of pressure, $P^{n+3/2,k+1}$.

*Step 5: Pressure correction.* Requiring that the continuity equation be satisfied at the new time step leads to an equation for a correction to the pressure field that is similar to the pressure-correction equation for incompressible flow. The procedure is derived for

the general case of $\overline{\overline{P}^t}^{t*}$. The case of $\overline{\overline{P}^t}^t$ is recovered if $\epsilon$ is set to zero in the following procedure. First, provisional corrections are added to the momentum per unit volume and the pressure,

$$g_i^{n+1,k+1} = \tilde{g}_i^{n+1,k+1} + \delta g_i, \quad P^{n+3/2,k+1} = P^{n+3/2,k} + \delta P. \tag{17}$$

These expressions are substituted into the momentum equations. To focus on the pressure terms, the convective and viscous terms are grouped into a generic term, R:

$$\begin{aligned}\frac{\tilde{g}_i^{n+1,k+1} + \delta g_i - g_i^n}{\Delta t} = -\delta_{x_i}\Bigg[&\left(\frac{1}{4} - \epsilon\right) P^{n-1/2} + \frac{1}{2} P^{n+1/2} \\ &+ \left(\frac{1}{4} + \epsilon\right)\left(P^{n+3/2,k} + \delta P\right)\Bigg] + R.\end{aligned} \tag{18}$$

Next this equation is split into a predictor and a corrector part:

$$\frac{\tilde{g}_i^{n+1,k+1} - g_i^n}{\Delta t} = -\delta_{x_i}\left[\left(\frac{1}{4} - \epsilon\right) P^{n-1/2} + \frac{1}{2} P^{n+1/2} + \left(\frac{1}{4} + \epsilon\right) P^{n+3/2,k}\right] + R, \tag{19}$$

$$\delta g_i = -\left(\frac{1}{4} + \epsilon\right) \Delta t \delta_{x_i}(\delta P). \tag{20}$$

Equation (19) is what was advanced for $\tilde{g}_i^{n+1,k+1}$ in step 4. Taking the divergence of Eq. (20) gives a Poisson equation for pressure:

$$\delta_{x_i}\left[\delta_{x_i}(\delta P)\right] = \frac{1}{\left(\frac{1}{4} + \epsilon\right) \Delta t} \delta_{x_i}\left(\tilde{g}_i^{n+1,k+1} - g_i^{n+1,k+1}\right). \tag{21}$$

Continuity at $t^{n+1}$ is enforced by substituting for $\delta_{x_i}(g^{n+1,k+1})$:

$$\delta_{x_i}\left[\delta_{x_i}(\delta P)\right] = \frac{1}{\left(\frac{1}{4} + \epsilon\right)\Delta t}\left[\delta_t(\rho)|^{n+1} + \delta_{x_i}\left(\tilde{g}_i^{n+1,k+1}\right)\right]. \tag{22}$$

The $\delta_t(\rho)|^{n+1}$ term is approximated using the known density at $t^{n+1/2}$ and an estimate for the density at $t^{n+3/2}$, which is obtained by adding the current estimate of the density at this time, $\tilde{\rho}^{n+3/2,k+1}$, and a term which accounts for the effect that the pressure correction $\delta P$ will have on the density at $t^{n+3/2}$:

$$\delta_t(\rho)|^{n+1} \approx \frac{\tilde{\rho}^{n+3/2,k+1} - \rho^{n+1/2}}{\Delta t} + \frac{1}{\Delta t} \left.\frac{\partial \rho}{\partial P}\right|_h \delta P. \tag{23}$$

Substituting Eq. (23) into Eq. (22) yields a Helmholtz equation for the pressure correction, $\delta P$:

$$\begin{aligned}&\delta_{x_i}\left[\delta_{x_i}(\delta P)\right] - \frac{1}{\left(\frac{1}{4} + \epsilon\right)\Delta t^2} \left.\frac{\partial \rho}{\partial P}\right|_h \delta P \\ &\quad = \frac{1}{\left(\frac{1}{4} + \epsilon\right)\Delta t}\left[\frac{\tilde{\rho}^{n+3/2,k+1} - \rho^{n+1/2}}{\Delta t} + \delta_{x_i}\left(\tilde{g}_i^{n+1,k+1}\right)\right].\end{aligned} \tag{24}$$

This Helmholtz equation is solved for $\delta P$, which is used to determine $g_i^{n+1,k+1}$ and $P^{n+3/2,k+1}$ from Eqs. (17) and (20). Notice that the magnitude of the Helmholtz term is proportional to $\frac{\partial \rho}{\partial P}\big|_h$ and inversely proportional to $\Delta t^2$. Since the number of iterations required to solve a Helmholtz equation decreases as the magnitude of the Helmholtz term increases, the time step and the choice of scalar will affect the performance of the Helmholtz solver. In the limit of large time step, the Helmholtz equation will become approximately equal to the Poisson equation that would be solved in the incompressible pressure-correction method.

*Step 6: Evaluate equation of state.* The density is again evaluated from the equation of state, using the more recent estimate of pressure:

$$\rho^{n+3/2,k+1} = \rho\left(P^{n+3/2,k+1}, h^{n+3/2,k+1}\right). \tag{25}$$

The iteration loop in steps 2 through 6 is repeated either for a fixed number of iterations or until some desired convergence criteria has been met.

There are several important features to note about this iterative process. First, the source term in Eq. (24) is proportional to the residual of Eq. (9), the continuity equation. This means that, as $\delta P$ converges to zero, the left side of Eq. (24) becomes zero, and Eq. (9) is satisfied. As $\delta P$ converges to zero, the pressure gradient terms in the momentum equations and the pressure terms in the enthalpy equation have also been treated implicitly. Second, the choice of which partial derivative of density with respect to pressure to use in Eqs. (23) and (24) does not affect the converged solution, since $\delta P$ will converge to zero [4]. It may, however, affect the convergence rate; therefore, it should be chosen appropriately. For example, evaluation of the partial derivative of density with respect to pressure at a constant value of the enthalpy, $h$, is appropriate, because enthalpy is constant during this portion of the iteration loop. The determination of the new value of density can be thought of as occurring in two parts. First, in steps 2 and 3, the density is updated to account for a change in enthalpy, $h$, at constant pressure. Then, in steps 5 and 6, the density is updated to account for a change in pressure at a constant enthalpy. Using this reasoning, if Eq. (12) is replaced by an equation for a different scalar, the partial derivative of density with respect to pressure is evaluated at a constant value of that scalar. For example, if an entropy equation replaces the enthalpy, the partial derivative of density with respect to pressure in Eq. (24) would be $\frac{\partial \rho}{\partial P}\big|_s$.

## 3. ANALYSIS OF THE SCHEME FOR SMALL-AMPLITUDE (LINEAR) ACOUSTICS

The properties of the method can be determined analytically in the case of one-dimensional small-amplitude (linear) acoustics when the scheme is implemented on a uniform Cartesian mesh. Performance on a nonuniform grid will be different, and the results derived here cannot be directly applied to that case. In the following analysis, it is shown that the numerical method does not artificially attenuate or amplify acoustic waves. An expression is also derived for the frequency at which acoustic waves oscillate in the numerical solution, and this is compared to the frequency obtained from the analytical solution. This analysis demonstrates some desirable properties of the method and provides a means of determining the resolution necessary to accurately represent waves of interest. This analysis is performed for implementation of the method with $\overline{\tilde{P}^t}^t$ used in the momentum equation. If $\overline{\tilde{P}^t}^{t*}$ is used

to remove unphysical oscillations at small scales, the method will be dissipative, but the amount of dissipation can be controlled by changing the value of $\epsilon$ in Eq. (14), and in the limit of $\epsilon$ approaching zero, the properties of the method approach what is found in this section. In the case of linear acoustics, the governing equations reduce to

$$\frac{\partial \rho'}{\partial t} = -\frac{\partial (\rho u)'}{\partial x}, \tag{26}$$

$$\frac{\partial (\rho u)'}{\partial t} = -\frac{\partial P'}{\partial x}, \tag{27}$$

$$\rho' = \frac{1}{c^2} P', \tag{28}$$

where the prime symbol indicates deviation from the mean value. Differentiating and combining these equations results in a wave equation for the pressure fluctuations:

$$\frac{\partial^2 P'}{\partial t^2} = c^2 \frac{\partial^2 P'}{\partial x^2}. \tag{29}$$

On a periodic domain, the solution to this equation is

$$P'(x, t) = P'_0 \exp[i(\omega t \pm kx)], \quad \omega = kc, \tag{30}$$

where $\omega$ is the frequency and $k$ is the wavenumber of the acoustic wave.

In this one-dimensional, linear case, the numerical scheme reduces to

$$\delta_t(P') = -c^2 \delta_x(g'), \tag{31}$$

$$\delta_t(g') = -\delta_x\left(\overline{\overline{P'}^t}^t\right). \tag{32}$$

Applying the $\delta_t$ operator to Eq. (31) and applying the $\delta_x$ operator to Eq. (32) yields

$$\delta_t[\delta_t(P')] = -c^2 \delta_t[\delta_x(g')], \tag{33}$$

$$\delta_t[\delta_x(g')] = -\delta_x\left[\delta_x\left(\overline{\overline{P'}^t}^t\right)\right]. \tag{34}$$

Substituting Eq. (34) into Eq. (33) gives the discrete version of the wave equation:

$$\delta_t[\delta_t(P')] = c^2 \delta_x\left[\delta_x\left(\overline{\overline{P'}^t}^t\right)\right]. \tag{35}$$

The propagation of acoustic waves by the discrete equations can now be analyzed. Since the problem is linear, each mode is independent of other modes; therefore, the analysis can be performed for a single mode having wavenumber $k$. Accounting for the spatial discretization, the numerical solution can be described by

$$\delta_t[\delta_t(\hat{P}')] = -c^2 (k')^2 \left(\overline{\overline{\hat{P}'}^t}^t\right). \tag{36}$$

In this equation, a spatial Fourier transform of Eq. (35) has been performed, and the Fourier coefficient of pressure for the wavenumber $k$ is indicated by $\hat{P}$. The modified wavenumber $k'$ of the $\delta_x[\delta_x(\,)]$ operator [20, 21] is defined by the relationship $\delta_x[\delta_x(e^{ikx})] = -k'^2 e^{ikx}$.

For a given spatial discretization scheme, the product $k'\Delta x$ is a known function of $k\Delta x$. For the central difference scheme used here this relationship is

$$k'\Delta x = \sqrt{(2 - 2\cos(k\Delta x))}. \tag{37}$$

In conventional notation, Eq. (36) can be written

$$\frac{(\hat{P}')^{n+3/2} - 2(\hat{P}')^{n+1/2} + (\hat{P}')^{n-1/2}}{\Delta t^2} = -c^2(k')^2 \frac{(\hat{P}')^{n+3/2} + 2(\hat{P}')^{n+1/2} + (\hat{P}')^{n-1/2}}{4}. \tag{38}$$

Assuming solutions of the form $(\hat{P}')^m = \hat{P}'_0\sigma^m$ and substituting into Eq. (38) results in a quadratic equation for $\sigma$, we get

$$\left[1 + \frac{(\Delta t c k')^2}{4}\right]\sigma^2 + \left[-2 + \frac{(\Delta t c k')^2}{2}\right]\sigma + \left[1 + \frac{(\Delta t c k')^2}{4}\right] = 0. \tag{39}$$

The error of a numerical scheme can be quantified by the error in amplitude introduced at each time step, which is related to the magnitude of $\sigma$, and the error in phase introduced at each time step, which is related to the phase of $\sigma$.

Solving Eq. (39) for $\sigma$ yields

$$\sigma = \frac{\left[\sqrt{2} \pm i\frac{\Delta t c k'}{\sqrt{2}}\right]^2}{2 + \frac{(\Delta t c k')^2}{2}}. \tag{40}$$

The analysis will be continued by examining only the root of sigma which has the positive sign in the numerator. Analysis of the other root is similar and yields the same results.

An attractive property of this method is that the magnitude of $\sigma$ is equal to one,

$$|\sigma| = 1, \tag{41}$$

regardless of the values of $k'$ or $\Delta t$, provided that $k'$ is real, which is true for the present spatial discretization scheme and any other centered scheme. This means that acoustic waves are not artificially amplified or attenuated by the numerical method, regardless of the spatial grid spacing or the size of the time step used.

The change in phase, $\Delta\theta$, of the numerical solution for $\hat{P}'$ at each time step is given by

$$\Delta\theta = \tan^{-1}\left[\frac{\mathrm{Im}(\sigma)}{\mathrm{Re}(\sigma)}\right] = \tan^{-1}\left[\frac{2\Delta t c k'}{2 - \frac{1}{2}(\Delta t c k')^2}\right]. \tag{42}$$

In this equation, the inverse tangent function is defined to have a range from 0 to $\pi$, instead of the usual $-\pi/2$ to $\pi/2$. This is done to ensure that values of sigma with positive imaginary parts and negative real parts are properly described as being in the second quadrant by this inverse tangent function. Defining the frequency of the numerical solution $\omega_n$ to be $\Delta\theta/\Delta t$, a ratio of the frequency of the numerical solution $\omega_n$ to the actual frequency $\omega$ can be obtained. Inserting this definition of $\omega_n$ into Eq. (42) results in

$$\frac{\omega_n}{\omega} = \frac{1}{(\mathrm{CFL})(k\Delta x)} \tan^{-1}\left[\frac{2(\mathrm{CFL})(k'\Delta x)}{2 - \frac{1}{2}((\mathrm{CFL})(k'\Delta x))^2}\right], \tag{43}$$

where the CFL number, based on the acoustic speed, is

$$\mathrm{CFL} = \frac{c\Delta t}{\Delta x}. \tag{44}$$

The results of this analysis can be used to determine the resolution required for simulation *a priori*. For example, on a spatial grid on which the shortest acoustic waves of interest have 20 grid points per wavelength ($k\Delta x = \pi/10$), Eq. (43) can be used to determine that the CFL number must be 2.48 or less if $\omega_n/\omega$ is required to be greater than or equal to 0.95 for the wavelengths of interest. This topic will be discussed further in the context of an actual LES in Section 4.4.

## 4. RESULTS

### 4.1. *Linear Acoustics*

The properties of the method for linear acoustics derived in Section 3 have been verified by numerical simulations of the Euler equations for the case of small-amplitude acoustic waves in a periodic domain. The Euler equations provide a more difficult test of the stability of the method, since they contain no viscous or diffusive terms to damp oscillations that may be present. In this and all other numerical tests, constant values of specific heat have been assumed. In this, as in all other simulations except for the LES of Section 4.4, $\overline{\bar{P}^t}^t$ is used with no added dissipation. This point will be discussed further in Section 4.4. In the first test, the algorithm as presented in Section 2 has been used to time advance acoustic waves from an initial condition of a small-amplitude ($u_{\max}/c = 10^{-6}$) sinusoidal velocity disturbance on a periodic domain. An entropy equation was solved instead of the enthalpy equation presented in Section 2. In this case the algorithm requires only one iteration per time step, since the equations are approximately linear, and entropy is constant. If the enthalpy equation had been used, the method may have required more iterations per time step, but it would have, otherwise, been equivalent. Since the acoustic waves have small amplitude, the full set of discrete equations reduces approximately to Eqs. (31) and (32), and these simulations can be used to test the relationships determined in the analysis. Results are compared to the barely implicit correction (BIC) method [2], which is the only other method of which the authors are aware that avoids the acoustic CFL limitation and for which published data for the time accurate simulation of acoustic waves are available.

The amplitude of the acoustic waves has been found to remain constant in the numerical simulations, verifying Eq. (41). In Fig. 1 the magnitude of sigma has been plotted versus spatial resolution, which is measured by the product of the wavenumber $k$, of the acoustic wave and the grid spacing $\Delta x$. In this plot, results from the proposed Helmholtz method are compared to results from the BIC method for simulations performed at $\mathrm{CFL} = 0.5$. It is clear that the Helmholtz method does not alter the amplitude of acoustic waves, while the BIC method causes significant attenuation of nearly all scales of acoustic waves. Although not shown, at larger CFL numbers the Helmholtz method still causes no attenuation of acoustic waves, while the attenuation caused by the BIC method becomes even greater.

The frequency of the acoustic waves in the numerical simulations has also been compared to the theoretical predictions and to the BIC method. Figure 2 is a plot of the ratio of the

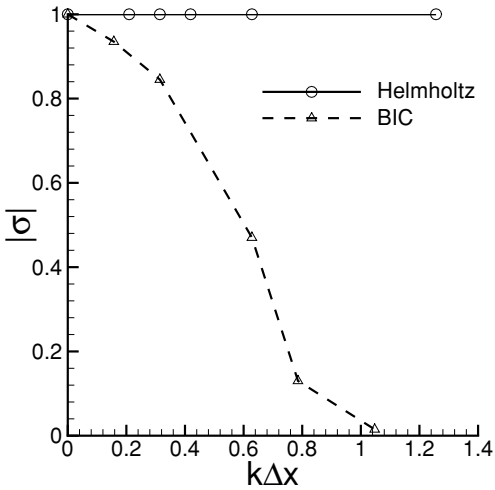


**FIG. 1.** Comparison of amplification/attenuation of acoustic waves by the Helmholtz and BIC methods.

frequency of the numerical solution to the frequency of the analytical solution, $\omega_n/\omega$, versus the spatial resolution $k\Delta x$. Results from the proposed Helmholtz method are compared to theoretical predictions and to results from the BIC method [2] for simulations performed at CFL $= 0.5$ and 2. It can be seen that the theoretical predictions of the numerical frequency are correct and that the Helmholtz method represents the frequency of acoustic waves more accurately than the BIC method. It is also possible to collapse the theoretical predictions for the frequency of the numerical solution given in Eq. (43) into a single curve. Figure 3 contains a plot of the theoretical prediction of $(\omega_n/\omega)(\text{CFL})(k\Delta x)$ versus $(\text{CFL})(k'\Delta x)$ along with data from the numerical tests.

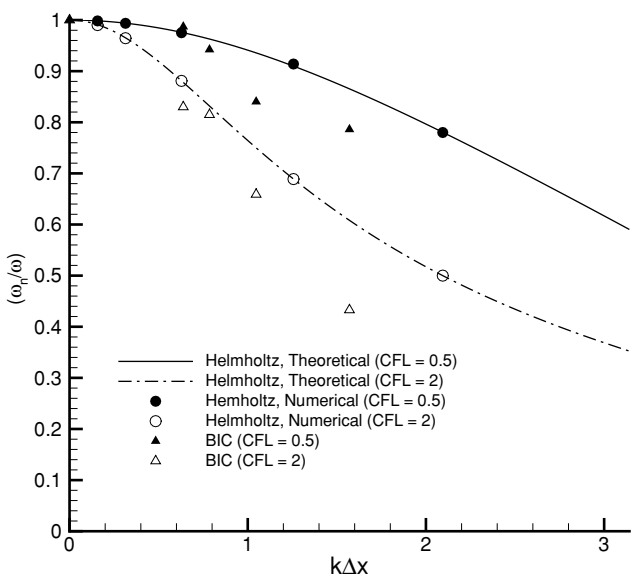


**FIG. 2.** Comparison of dispersion relationship to BIC method.

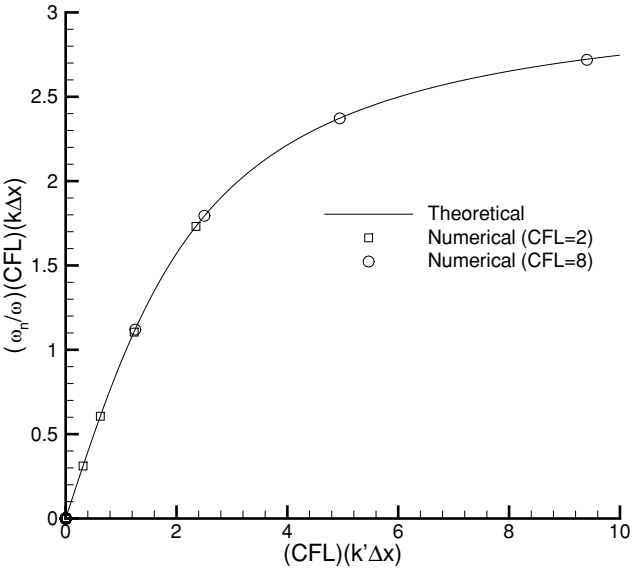


**FIG. 3.** Collapsed curve for dispersion relationship of Helmholtz method.

The method's property of preserving the amplitude of acoustic modes has also been tested for a two-dimensional case. In this test, a rectangular domain with solid-wall boundary conditions on three sides and a constant-pressure boundary condition on the remaining side has been initialized to contain a small-amplitude acoustic mode consisting of a three-quarter wave in the $x$ direction and a full wavelength in the $y$ direction. Contours of pressure in this acoustic mode are shown in Fig. 4. The grid consists of 48 equally spaced points in the $x$ direction and 32 equally spaced points in the $y$ direction, and the time step is such that the CFL numbers are 2.21 and 8.83 in the $x$ and $y$ directions, respectively. In Fig. 5 the pressure near the pressure antinode at the left boundary is plotted as a function of time. This is done twice, once at the beginning of the simulation and once after about 100 periods of oscillation. In this plot the fluctuating pressure normalized by the mean pressure is plotted versus the nondimensionalized time $\omega t$, where $\omega$ is the analytical frequency at which the mode should oscillate. This plot shows that the amplitude of pressure fluctuations does not change significantly over the course of about 100 periods. Analysis of the data does show that the amplitude of oscillation has actually decreased by about 2.8% between the time $\omega t = 5$ and $\omega t = 95$. By accounting for the number of time steps between these two times, these data can be used to calculate that the absolute value of $\sigma$, which was shown analytically to be unity in Eq. (41), is actually 0.99993 in this simulation. This discrepancy is small enough to be neglected in nearly all cases of interest.

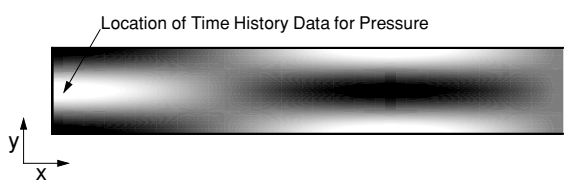


**FIG. 4.** Shape of pressure fluctuations in two-dimensional acoustic mode.

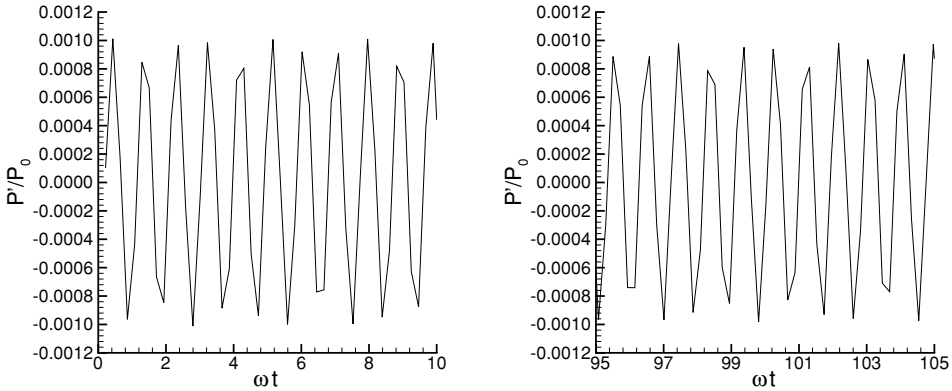


**FIG. 5.** Time history of pressure fluctuations.

### 4.2. *Order of Accuracy*

Convergence rates of the proposed Helmholtz method have also been verified by numerical tests. In these tests, the algorithm as presented in Section 2 has been used to time advance the Euler equations on a periodic domain of length $L$. The initial condition for velocity is $u(x) = 0.1c + 0.1c \sin(2\pi x/L)$, where $c$ is the sound speed. Pressure is initially constant ($P = P_0$), while entropy initially varies according to $s = s_0 + 0.1c_p \sin(2\pi x/L)$; therefore, density varies accordingly to satisfy the equation of state. There is also a heat input per unit volume, $Q = 0.1\gamma c P_0 \cos(2\pi x/L)/[(\gamma - 1)L]$. Figures 6 and 7 show the error $\epsilon$ in both the velocity and pressure, measured at $x = L/2$ and $t = L/c$, as functions of time step and spatial grid size. The data in the figures shown here were generated by implementing the method with entropy as the scalar. Although not shown, the method has also been confirmed to be second-order accurate for both velocity and pressure when the scalar equation is solved for enthalpy. These figures show that the method is second-order in both space and time as expected. It can be formally shown that the method is second-order accurate in time as long as at least two iterations are performed. In the case of two iterations, the method is actually a second-order Runge–Kutta method. To get the stability

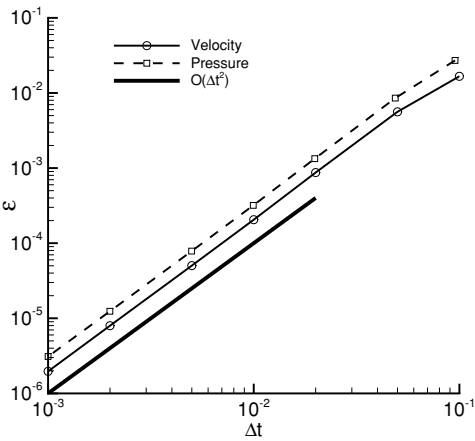


**FIG. 6.** Temporal convergence of Helmholtz method.

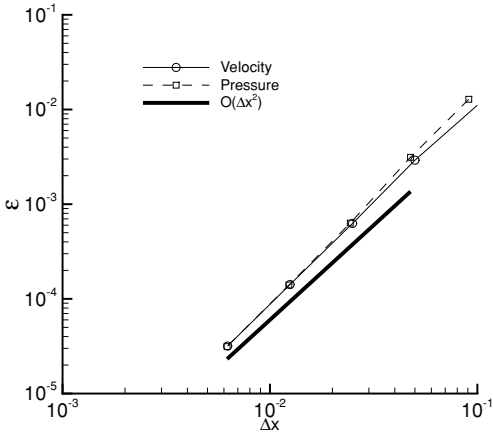


**FIG. 7.** Spatial convergence of Helmholtz method.

properties of the implicit method, however, the iteration process must be continued until convergence.

### 4.3. *One-Dimensional Model Combustor*

One important application in which the interaction of low-frequency acoustic waves with other flow phenomena at low Mach number is acoustic combustion instability in gas turbine combustors. Therefore, a set of simulations intended to provide a simple model for combustion problems has also been performed. The purpose of these simulations is to assess the performance of the method in the range of Mach numbers and density ratios, $\rho_{\max}/\rho_{\min}$, of interest in gas turbine combustors. In this test the Euler equations have been solved on a one-dimensional domain from $x = 0$ to $L$. At $x = 0$ the velocity has been specified to vary sinusoidally in time about a mean value, while entropy has been specified to be constant. The pressure at $x = L$ has also been specified to be constant. There is heat input to the fluid to model the heat release in the combustion process. This heat input is constant in time and is a parabolic function of $x$ ($Q(x) = 4Q_{\max}[x(1-x)]$). In these tests the initial condition for the simulation is the solution to the steady problem, which has no sinusoidal variation of the velocity at the inlet. The magnitude of the sinusoidal variation in velocity at the inlet ranged from zero to $0.1c$. This inlet variation results in acoustic waves, which propagate through the domain. In these tests the Mach number ranged from 0 to about 0.3, while the density ratio ranged from 0 to about 7. These parameter values are in the range that is expected in a gas turbine combustor simulation.

Sample solutions from a simulation for which the mean Mach number at the inlet is 0.1, the magnitude of the sinusoidal variation of the inlet velocity is $0.1c$, and for which the density ratio is 5.41 are shown in Fig. 8. In this figure the deviation of velocity from the mean, $u'(x)$, is plotted versus the spatial coordinate for four different times. Solutions from the Helmholtz method using 70 and 180 spatial grid points have both been computed using time steps such that the convective CFL number is between 0.9 and 1.0. In these simulations the CFL number based on the sum of the acoustic and convective velocities, which would limit the time step in an explicit calculation, was between 4.3 and 4.5. These results are compared to the "exact" solution, which is actually a well-resolved numerical

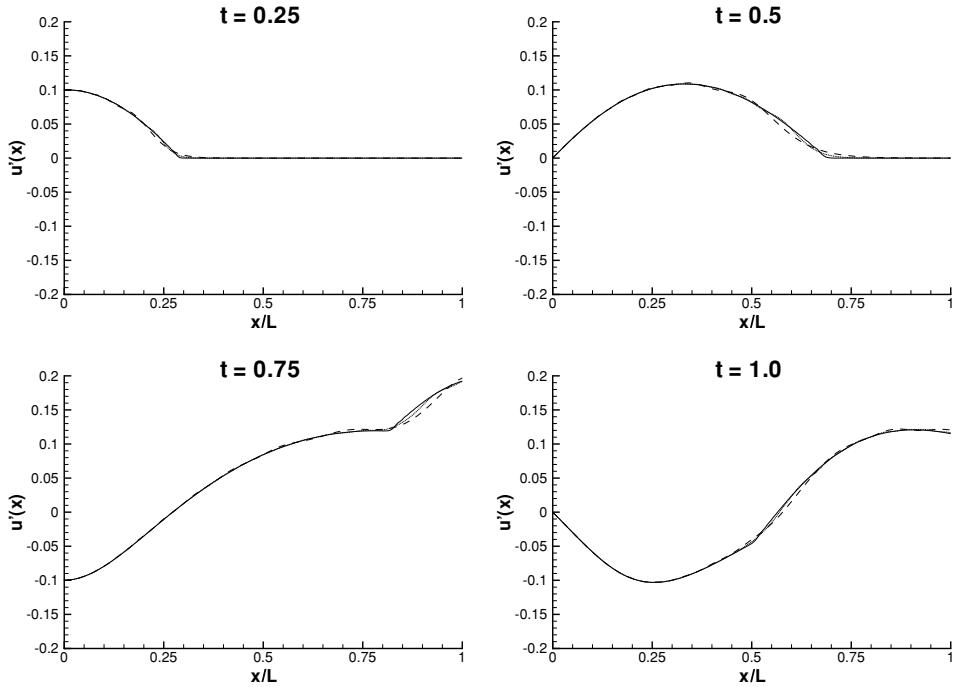


**FIG. 8.** Sample solutions of model combustor problem; $N = 70$ (– –), $N = 180$ (· · ·), "exact" (—).

solution from a traditional explicit method for compressible flow. The results demonstrate the successful use of the Helmholtz pressure-correction method in a case with large density variation.

### 4.4. *Large Eddy Simulation*

Finally, the method has been implemented into a large eddy simulation. The LES is of the nonreacting case of the experiments of Besson *et al.* [22]. In this experiment, the flow from two fully developed turbulent channels forms a mixing layer just upstream of a sudden expansion. This flow has previously been simulated by Duchamp de Lageneste and Pitsch [23] using an incompressible flow solver. The Mach number at the inlet is about 0.04; therefore, a significant efficiency gain can be achieved using the Helmholtz pressure-correction method. A contour plot of the streamwise velocity taken from the LES performed using the Helmholtz pressure-correction method is shown in Fig. 9.

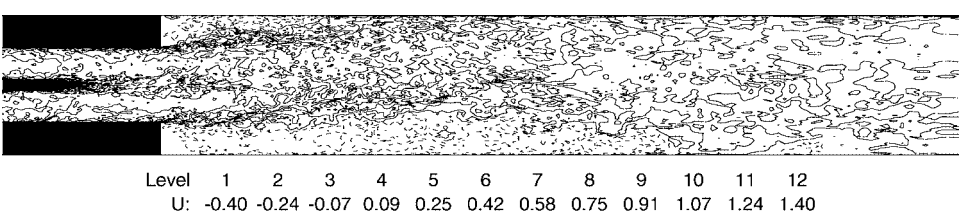


**FIG. 9.** Instantaneous contours of streamwise velocity from LES performed with Helmholtz pressure correction method (Dashed lines represent negative values.)

Boundary conditions for this simulation are those of Poinsot and Lele [24], which are based on a characteristic analysis of the Navier–Stokes equations. At the outlet, the amplitude $\mathcal{L}_1$ of the incoming acoustic wave is found by the relation

$$\mathcal{L}_1 = K_{\text{out}}(P(x, y, z, t) - P_0). \tag{45}$$

At the inlet, entropy is set to a constant, thus setting the amplitude of the incoming entropy wave to zero. The wall-normal component of velocity, $v$, and the spanwise component, $w$, are taken from a separate incompressible LES of turbulent channel flow. The streamwise component, $u$, is found by using the relation

$$\mathcal{L}_5 = K_{\text{in}}(U(x, y, z, t) - U_{\text{target}}(x, y, z, t)). \tag{46}$$

This relationship is similar to Eq. (45) and is discussed by Schönfeld and Poinsot [25]. In this equation, $L_5$ is the amplitude of the incoming acoustic wave. The target velocity $U_{\text{target}}$ is also taken from the incompressible LES from which $v$ and $w$ are taken. Once $\mathcal{L}_5$ is determined, the actual velocity at the inlet can be found according to Poinsot and Lele [24]. The relationships in Eqs. (45) and (46) are meant to allow the approximate specification of the values of flow variables at the boundaries, while still allowing acoustic energy to exit the domain through the boundary. If streamwise velocity at the inlet and pressure at the outlet are specified independently of the variables within the domain, all acoustic energy reaching the boundary will be reflected and large-amplitude acoustic modes will exist within the domain. If Eqs. (45) and (46) are used, and the values of $K_{\text{in}}$ and $K_{\text{out}}$ are chosen to be too large, too little acoustic energy will be allowed to leave the domain and large-amplitude acoustic modes will still exist.

The efficiency of the method is found to be as expected when used to perform the LES. Unlike the tests of Section 4.3 there is a large discrepancy in the time steps allowed by the convective CFL restriction and that which would be allowed by the acoustic CFL restriction. This occurs in the near-wall region, due to mesh stretching in the wall normal direction. In this region the wall-normal velocity also becomes small, but the acoustic velocity remains large, resulting in an acoustic CFL number which is much larger than the convective CFL number and more significant efficiency gains to be achieved if the acoustic CFL restriction is removed. The simulation is performed on a grid of $256 \times 128 \times 32$ grid points in the streamwise ($x$), wall-normal ($y$), and spanwise ($z$) directions respectively. The grid is significantly stretched in the wall-normal direction with adjacent grid cells differing in width by up to 28%. This amount of grid stretching is quite high and demonstrates the robustness of the method with respect to stretched grids. Except for a decrease by a factor of 2 in the number of points in the spanwise direction, this is the same grid which Duchamp de Lageneste and Pitsch used to resolve turbulent scales in their incompressible simulation. The time step used is $0.02H/U_{\text{ch}}$, where $H$ is the height of each channel upstream of the splitter plate, and $U_{\text{ch}}$ is the mean streamwise velocity within each channel. This is the same time step used in the incompressible simulations of Duchamp de Lageneste and Pitsch and results in acoustics CFL numbers as large as 40 in the wall-normal direction. The simulation required four iterations at each time step. Within each iteration, the Helmholtz solver was found to require about 22% of the time required for the iteration. This means that each time step requires about 2.6 times more time than an explicit method, assuming that the explicit method requires two iterations to achieve second-order temporal accuracy and that the explicit advancement of the continuity equation in the explicit solver requires negligible

**TABLE I**

**Estimate of Dispersion Error for Acoustic Modes Having Wavelength in the *x* Direction of One-Fifth of the Streamwise Distance from the Expansion Plane to the Exit Plane**

| | Min $\Delta x$ | Max $\Delta x$ |
|---|---|---|
| $\Delta x$ | 0.0545 | 0.3254 |
| $k\Delta x$ | 0.0685 | 0.409 |
| $k'\Delta x$ | 0.0685 | 0.406 |
| CFL | 10.1 | 1.70 |
| $\omega_n/\omega$ | 0.962 | 0.956 |

time compared to the solution of the Helmholtz equation. Assuming that the explicit method would be limited to an acoustic CFL number of 1, the Helmholtz pressure-correction method requires about 15 times less computational effort than the explicit solver would require for this LES.

In this LES, dissipation is introduced by using $\overline{\overline{P}^t}^{t*}$ as defined in Eq. (14) in the pressure gradient term of the momentum equation. Without introducing this dissipation, unphysical small-scale oscillations are found in the scalar variables. In the previous numerical tests that have been presented, this dissipation was not required, since there were no scales of the order of the smallest scales resolvable by the grid. Turbulent calculations, however, will inevitably have such scales present and, therefore, are likely to require such dissipation to prevent unphysical oscillations. For the time step used in this simulation, $\epsilon$ in Eq. (14) was chosen to be 0.005. This value is very small compared to the leading order coefficient of 0.25; therefore, the damping of larger scales is expected to be negligible.

The effects of dispersion have been estimated. Although Eq. (43) is not exact due to the nonuniform grid and the presence of $\epsilon$, it can be used to estimate the effects of dispersion on the acoustic modes of interest in the LES. By inserting maximum and minimum grid spacings in both the $x$ and $y$ directions into Eq. (43) it is estimated that $\omega_n/\omega > 0.95$ for acoustic modes having wavelength in the $x$ direction greater than one-fifth of the streamwise distance from the expansion plane to the exit and for modes having wavelength in the $y$ direction on the order of the channel width downstream of the expansion. Tables I and II provide more details about these estimates. In Table I a wavelength of one-fifth of the

**TABLE II**

**Estimate of Dispersion Error for Acoustic Modes Having Wavelength in the *y* Direction Equal to the Channel Height Downstream of the Expansion Plane**

| | Min $\Delta y$ | Max $\Delta y$ |
|---|---|---|
| $\Delta y$ | 0.0139 | 0.130 |
| $k\Delta y$ | 0.0198 | 0.186 |
| $k'\Delta y$ | 0.0198 | 0.186 |
| CFL | 39.7 | 4.23 |
| $\omega_n/\omega$ | 0.953 | 0.951 |

streamwise distance from the expansion plane to the exit plane is assumed, and in Table II a wavelength equal to the channel height downstream of the expansion plane is assumed. These estimates show that even though the CFL number is as large as 40, the acoustic waves of interest do not have excessive dispersion error.

## 5. CONCLUSIONS

A pressure-correction method for simulation of the compressible Navier–Stokes equations for which the time step is limited only by a convective CFL condition is presented. The method is proposed for simulating flows at low Mach number in which the interaction between long-wavelength acoustic modes and other flow phenomena is of interest. The method is similar to the pressure-correction method for incompressible flow, but it requires an iterative process at each time step. An analysis of the method in the case of linear acoustics is presented. The method is shown to cause no artificial attenuation of acoustic waves, regardless of time step or grid size. An analytical formula is derived for the frequency at which acoustic waves will oscillate in the numerical solution. This analysis has been verified by numerical tests. In turbulence simulations, it may be desirable to add dissipation to the method to prevent unphysical point-to-point oscillations in the flow variables due to the presence of short-wavelength acoustic modes which otherwise would not be dissipated by the method. A provision for adding dissipation, in a manner which can be controlled to have the desired effect on small scales without overly damping long-wavelength acoustic modes, is presented. As long as the method does not overly damp the long-wavelength modes, which are the ones of interest in the simulations for which the method is designed, the method will be able to capture the interaction between these acoustic modes and other phenomena in the simulation.

Simple one- and two-dimensional tests confirm the properties of the method when implemented without dissipation. The method is also shown to be second-order accurate in both time and space, and it is shown to work in a simulation of a one-dimensional model problem with heat input.

The method is shown to result in large efficiency gains when performing LES at low Mach number. In the LES there is a large discrepancy in acoustic and convective CFL numbers, due to near-wall grid refinement; therefore, the avoidance of the acoustic CFL condition leads to much larger allowable time steps. This difference in allowable time steps will, of course, depend on Mach number and the spatial grid. In the LES performed here, time steps taken were about 40 times larger than what would be allowed by an explicit method but required only about 2.6 times more effort per time step, resulting in about a factor of 15 reduction in computational expense.

## ACKNOWLEDGMENTS

This work has been partially supported by the Department of Energy though the Accelerated Strategic Computing Initiative. The authors also thank Professor Sanjiva Lele, Dr. Heinz Pitsch, and Dr. Laurent Duchamp de Lageneste for their helpful discussions.

## REFERENCES

1. G. Strang, On the construction and comparisons of difference schemes, *SIAM J. Numer. Anal.* **5**, 506 (1968).

2. G. Patnaik, R. H. Guirguis, J. P. Boris, and E. S. Oran, A barely implicit correction for flux-corrected transport, *J. Comput. Phys.* **71**, 1 (1987).
3. K. C. Karki and S. V. Patankar, Pressure based calculation procedure for viscous flows at all speeds in arbitrary configurations, *AIAA J.* **27**, 1167 (1989).
4. I. Demirdžić, Ž. Lilek, and M. Perić, A collocated finite volume method for predicting flows at all speeds, *Int. J. Numer. Methods Fluids* **16**, 1029 (1993).
5. H. Bijl and P. Wesseling, A unified method for computing incompressible and compressible flows in boundary-fitted coordinates, *J. Comput. Phys.* **141**, 153 (1998).
6. J. S. Shuen, K. H. Chen, and Y. H. Choi, A coupled implicit method for chemical non-equilibrium flows at all speeds, *J. Comput. Phys.* **106**, 306 (1993).
7. R. H. Pletcher and K. H. Chen, *On Solving the Compressible Navier–Stokes Equation for Unsteady Flows at Very Low Mach Numbers*, AIAA Paper 93-3368 (1993).
8. W. P. Wang, *Coupled Compressible and Incompressible Finite Volume Formulations for LES of Turbulent Flow with and without Heat Transfer*, Ph.D. thesis (Iowa State University, Ames, IA, 1995).
9. S. Venkateswaran and C. L. Merkle, *Dual Time Stepping and Preconditioning for Unsteady Computations*, AIAA Paper 95-0078 (1995).
10. L. D. Dailey and R. H. Pletcher, Evaluation of multigrid acceleration for preconditioned time-accurate Navier–Stokes algorithms, *Comput. Fluids* **25**, 791 (1996).
11. P. E. O. Buelow, D. A. Schwer, J. Feng, C. L. Merkle, and D. Choi, *A Preconditioned Dual-Time, Diagonalized ADI Scheme for Unsteady Computations*, AIAA Paper 97-2101 (1997).
12. I. Mary, P. Sagaut, and M. Deville, An algorithm for low Mach number unsteady flows, *Comput. Fluids* **29**, 119 (2000).
13. I. Mary, P. Sagaut, and M. Deville, An algorithm for unsteady viscous flows at all speeds, *Int. J. Numer. Methods Fluids* **34**, 371 (2000).
14. F. H. Harlow and J. E. Welch, Numerical calculation of time-dependent viscous incompressible flow of fluid with free surface, *Phys. Fluids* **8**, 2182 (1965).
15. Y. Morinishi, T. S. Lund, O. V. Vasilyev, and P. Moin, Fully conservative higher order finite difference schemes for incompressible flow, *J. Comput. Phys.* **143**, 90 (1998).
16. C. D. Pierce, *Progress-Variable Approach for Large-Eddy Simulation of Turbulent Combustion*, Ph.D. thesis (Stanford University, Stanford, CA, 2001).
17. I. Christie, D. F. Griffiths, A. R. Mitchell, and O. C. Zienkiewicz, Finite element methods for second order differential equations with significant first derivatives, *Int. J. Numer. Methods Eng.* **10**, 1389 (1976).
18. A. N. Brooks and T. J. R. Hughes, Streamline upwind/Petrov–Galerkin formulations for convection dominated flows with particular emphasis on the Navier–Stokes equations, *Comput. Methods Appl. Mech. Eng.* **32**, 199 (1982).
19. V. Casulli and D. Greenspan, Pressure method for the numerical solution of transient, compressible fluid flows, *Int. J. Numer. Methods Fluids* **4**, 1001 (1984).
20. P. Moin, *Fundamentals of Engineering Numerical Analysis* (Cambridge Univ. Press, Cambridge, UK, 2001).
21. S. K. Lele, Compact finite-difference schemes with spectral-like resolution, *J. Comput. Phys.* **103**, 16 (1992).
22. M. Besson, P. Bruel, J. L. Champion, and B. Deshaies, *Inert and Combusting Flows Developing over a Plane Symmetric Expansion: Experimental Analysis of the Main Flow Characteristics*, AIAA Paper 99-0412 (1999).
23. L. Duchamp de Lageneste and H. Pitsch, Progress in large-eddy simulation of premixed and partially-premixed turbulent combustion, in *CTR Annual Research Briefs* (Center for Turbulence Research, NASA Ames/Stanford University, 2001), p. 97.
24. T. J. Poinsot and S. K. Lele, Boundary conditions for direct simulations of compressible viscous flows, *J. Comput. Phys.* **101**, 104 (1992).
25. T. Schönfeld and T. Poinsot, Influence of boundary conditions in LES of premixed combustion instabilities, in *CTR Annual Research Briefs* (Center for Turbulence Research, NASA Ames/Stanford University, 1999), p. 73.